Phys. Status Solidi A **210**, No. 3, 474–479 (2013) / **DOI** 10.1002/pssa.201200653

physica status solidi a
www.pss-a.com
applications and materials science

MBE growth and applications of cubic AlN/GaN quantum wells

Donat J. As* **and Christian Mietze**

Department Physik, Universität Paderborn, Warburger Strasse 100, 33098 Paderborn, Germany

Received 5 September 2012, revised 21 November 2012, accepted 30 November 2012
Published online 28 December 2012

Keywords cubic AlN, GaN, interband and intersubband transitions, MBE, resonant tunneling

* Corresponding author: e-mail d.as@uni-paderborn.de, Phone: +49 5251 60 5838, Fax: +49 5251 60 5943

Molecular beam epitaxy (MBE) of cubic group III-nitrides is a direct way to eliminate polarization effects which inherently limit the performance of optoelectronic devices containing quantum well or quantum dot active regions. In this contribution, the latest achievement in the MBE of phase-pure cubic GaN, AlN, and AlN/GaN quantum wells will be reviewed. The structural, optical, and electrical properties of state of the art cubic nitrides and AlGaN/GaN will be presented. We show that no polarization field exists in cubic nitrides and demonstrate intersubband absorption at 1.55 μm in cubic AlN/GaN superlattices. Comparing the experimental results with simulations based on an effective-mass model the GaN/AlN conduction-band offset is demonstrated to be higher than 1.2 eV. The best fit with the experimental data is achieved for a conduction-band offset of 1.4 eV. Further the progress toward the fabrication of cubic GaN/AlGaN superlattices for terahertz applications will be discussed and our first experiments on cubic AlN/GaN resonant tunneling devices will be reported.

1 Introduction Group III-nitride-based opto-electronic and electronic devices, which are commercially available at the market, are grown along the polar *c* direction, which suffer from the existence of strong "built-in" piezoelectric and spontaneous polarization. This inherent polarization limits the performance of optoelectronic devices containing quantum well or quantum dot active regions. To get rid of this problem much attention has been focused on the growth of non- or semi-polar (Al,Ga,In)N. An alternative way to eliminate polarization effects is the growth of cubic (100) oriented III-nitride layers. However, since cubic GaN is metastable and no cubic GaN bulk material exists in nature, heteroepitaxy with all its drawbacks due to lattice mismatch is necessary to grow this material. Due to the low lattice mismatch to cubic GaN the substrate of choice for the growth of cubic III-nitrides is 3C-SiC (001).

In this contribution, the latest achievements in the molecular beam epitaxy (MBE) of phase-pure cubic GaN, AlN, and their alloys grown on 3C-SiC substrates is reviewed [1]. The structural and optical properties of cubic nitrides, cubic Al(Ga)N/GaN heterostructures, cubic GaN/Al(Ga)N multiple quantum wells (MQW) and superlattices (SL) will be shown [2], and the absence of polarization fields in cubic nitrides will be demonstrated [3]. Intersubband absorption and photoluminescence of cubic GaN/Al(Ga)N quantum wells is studied experimentally and theoretically over a wide spectral range. By changing the quantum well thickness it is possible to tune the intersubband absorption peak wavelength from 1.4 μm (214 THz) to 63 μm (4.76 THz). Comparing the experimental results with simulations based on the effective-mass model the GaN/AlN conduction-band offset is demonstrated to be higher than 1.2 eV [4]. The best fit with the experimental data is achieved for a conduction-band offset of 1.4 eV and for a GaN effective mass of $0.11 m_0$.

Resonant tunneling diodes (RTD) of cubic AlN/GaN show a pronounced negative differential resistance (NDR) at about 1.2 V with a peak-to-valley ratio (PVR) of 1.3–2.7 at room temperature [5]. The experimental data are in good agreement with calculated *I–V* curves showing only a small deviation of 0.3 V of the resonance peak voltage. We find a decrease of the PVR when the *I–V* characteristic is measured repeatedly with short time intervals between the voltage-cycles. However, the *I–V* characteristics can be recovered fully when the diodes are illuminated by UV-light indicating charge trapping in our devices.

2 Experimental The samples were grown by plasma assisted molecular beam epitaxy (PA-MBE) on a 10 μm thick 3C-SiC on Si(001) templates. This substrate has been

Table 1 Parameters of AlGaN/GaN MQW samples.

sample	QW thickness, nm	barrier thickness, nm	Al content in the barriers (%)	doping (cm^{-3})
A (1967)	2	3	100	5×10^{19}
B (1966)	3	3	100	1×10^{19}
C (1981)	5	3	100	1×10^{19}
D (1849)	12	15	5	2×10^{17}

chosen due to its good transparency both in the near infrared and in the far infrared spectral range. All quantum structures were grown at $T_{substrate} = 720\,^{\circ}C$. Growth was controlled by *in situ* reflection high energy electron diffraction (RHEED). The GaN layers were grown under 1 ML Ga-coverage, which was found to be the optimal growth condition for cubic GaN [3], while the AlN layers were grown under N-rich conditions [6]. During the superlattice structure growth was interrupted after each layer to evaporate excess metal from the surface. The thickness of the AlN layers was controlled by RHEED-intensity oscillations while the GaN growth rate was estimated from AlGaN growth oscillations and thickness measurements on the reference sample. Growth rate for AlN was 0.19 and 0.18 ML s^{-1} for GaN. For more details on the growth please refer to Ref. [1].

For photoluminescence and optical absorption measurements the samples consist of a 100 nm thick GaN buffer layer followed by 40 periods of GaN/Al(Ga)N QWs and a GaN cap layer. For samples A, B, and C the cap layer thickness is 7 nm and for sample D this thickness is 30 nm. The QWs are n-doped with Si in order to populate the ground electronic state. The QW thickness is varied in order to shift the intersubband (ISB) fundamental e_1–e_2 transition energy. The structural quality of the GaN/Al(Ga)N superlattices was assessed using X-ray diffraction. From the positions of additional superlattice satellites in ω–2θ scans of the symmetrical (002) reflection the lattice period of the superlattice structures was calculated. In addition, simulations for the X-ray measurements were performed using dynamical scattering theory [7]. Using X-ray simulations not only the lattice parameter but also the thicknesses of the individual layers can be determined. Good agreement between experimental and calculated data can only be achieved assuming the correct thicknesses for both QW and barrier layers. The QW and barrier thickness and the doping level are summarized in Table 1.

The samples were then characterized by UV photoluminescence (PL) spectroscopy. The excitation is provided with a cw frequency-doubled Ar^+ laser ($\lambda = 244$ nm) and the spectra are analyzed using a Jobin Yvon HR460 spectrometer equipped with a CCD camera.

3 Results and discussion

Due to the wide band gaps and the large band offsets between AlN and GaN this group of III-nitrides offer intersubband transitions in the technologically important infrared 1.3–1.5 μm spectral range. The growth of non-polar cubic GaN/AlN multi quantum well (MQW) structures on (001) oriented substrates will eliminate the detrimental strong spontaneous polarization fields, allowing easier design of the complex MQW structures with various quantum well widths as it is necessary for the QCL systems.

3.1 Optical and structural properties

The photoluminescence spectra at room temperature are shown in Fig. 1 for the four MQW samples. All emission energies are observed above the near band gap emission of cubic GaN and progressively redshift with increasing QW thickness. The measured energies are in good agreement with calculations done for a rectangular potential profile [3]. As expected for cubic nitride QWs, no evidence of internal field and of quantum confined Stark effect can be observed [8].

The inset in Fig. 1 shows a typical ω–2θ scan of sample B with the related simulation. The layer thicknesses deduced from X-ray diffraction for all samples are in good agreement with the nominal ones. Additionally the strain in the superlattice samples was investigated by reciprocal space maps of the asymmetrical (113) reflection (not shown here). For samples A, B, and C we find that the AlN layers are not fully strained on GaN. From the position of the SL reflexes we conclude that the SL structure has formed an average lattice constant between GaN and AlN meaning that the AlN layers are partially relaxed while the GaN is partially strained.

3.2 Intersubband absorption

For ISB absorption measurements, samples were polished in a multi-pass waveguide geometry with parallel facets inclined by 30° with respect to the substrate plane to avoid both the total internal reflection on the Si/SiC interface and to maximize the interaction of the electro-magnetic field with the dipole of

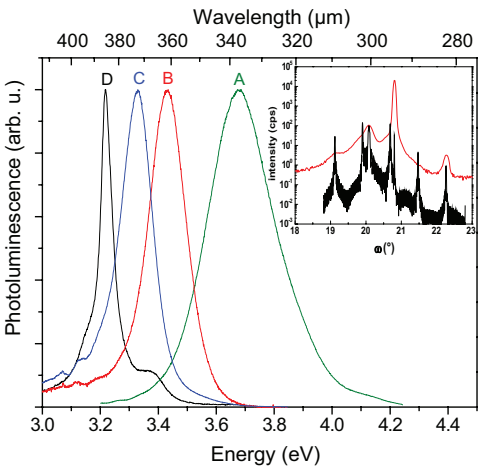

Figure 1 (online color at: www.pss-a.com) Room temperature PL spectra of four cubic AlN/GaN MQWs (samples A, B, C, and D listed in Table 1). Inset: X-ray diffraction ω–2θ spectrum of sample B and a corresponding simulation with nominal layer thicknesses (bottom curve).

the ISB transition (oriented along the growth axis). Infrared absorption measurements were performed at room temperature using a Fourier transform infrared spectrometer (FTIR). A typical transmission spectrum for TM- (p-) and TE- (s-) polarized light is shown in the inset to Fig. 2 and the spectrum is normalized by the response of the optical system. The oscillations observed in the spectrum arise from the Fabry–Perot interferences in the 10 μm thick SiC layer. The high energy cut-off corresponds to the absorption of the Si substrate whereas the low energy transmission drop at 0.21 eV corresponds to the two-phonon absorption of the SiC template. An absorption peak at 0.46 eV is observed for TM-polarized light which is a clear signature of an ISB resonance.

Figure 2 displays the ISB absorption spectra of three different samples together with the corresponding Gaussian fits. The absorption peaks are at 1.4 μm (sample A), 2.7 μm (sample B), and 4.1 μm (sample C), respectively. These data show that the broadening of the ISB absorption in cubic QWs is larger than in their hexagonal counterparts. For example, the full width at half maximum (FWHM) is 0.17 eV which is slightly higher than the typical broadening observed for hexagonal GaN/AlN QWs absorbing in the same spectral range (typically 60–100 meV in doped QWs [9, 10] and 40 meV in undoped samples [11]). In Ref. [12] the broadening is attributed to thickness fluctuations, interface roughness, and impurity scattering as in the case of GaAs/AlGaAs QWs. The large broadening in relatively wide cubic QWs may be due to fluctuations of the QW thickness which have a stronger influence on the transition energy in the case of cubic QW than in hexagonal QW, because internal electric fields in the latter confine the carriers and makes the transition energy almost thickness-independent [10].

3.3 Band alignment For a better understanding and fabrication of devices the conduction and valence band discontinuities of these heterostructures are badly needed. Presently only little research on the band offsets between zincblende GaN and AlN is done. Therefore, the measured interband and intersubband transition energies reported above are compared with calculated energies using a 1D Poisson-Schrödinger solver and a detailed *ab initio* approach. Intersubband transition energies in superlattices depend mainly on the conduction band offset (CBO) between quantum well and barrier material while interband transition energies depend on conduction and valence band discontinuities. For given band gap energies and structural properties of superlattice structures the calculated transition energies can be brought into agreement with measured values by variation of the ratio of CBO to valence band offset.

Figure 3 shows the calculated interband (full curves) and intersubband (dotted curves) transition energies as a function of the CBO for samples A, B, and C. The transition energies of the interband transitions are determined from photoluminescence measurements (open symbols) whereas the intersubband transition energies are obtained from the ISB absorption measurements (full symbols).

The quantum confinement in cubic QWs was modeled using an effective mass model. The PL and ISB transition energies of the QW structures were then calculated by self-consistently solving the Schrödinger and Poisson equations. These simulations allowed obtaining some material parameters, e.g., the electron effective mass in cubic GaN was estimated to be close to $0.11 m_0$ and the CB offset between GaN and AlN was found to be about 1.4 eV [4].

The valence-band offset (VBO) and the CBO were also calculated using an *ab initio* approach (calculating many-body corrections) within the *GW* approximation on top of hybrid-functional density functional theory calculations. A CBO of (1.4 ± 0.1) eV and a VBO of (0.5 ± 0.1) eV is obtained in good agreement with the values deduced from measured inter- and intersubband transition energies [2] (Fig. 4).

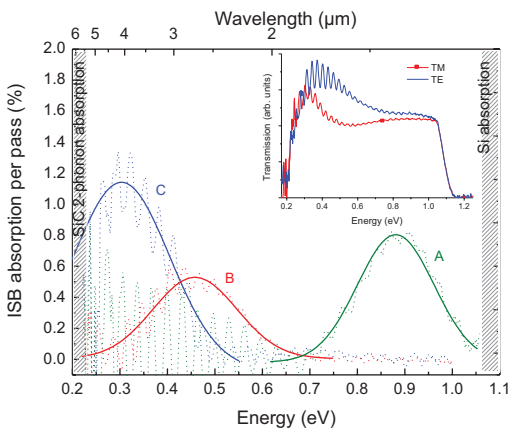

Figure 2 (online color at: www.pss-a.com) Room-temperature ISB absorption per pass in the active region of samples A, B, and C (dotted curves) and corresponding Gaussian fits (full curves). Inset: room temperature infrared transmission spectrum of sample B for TM- and TE-polarized light.

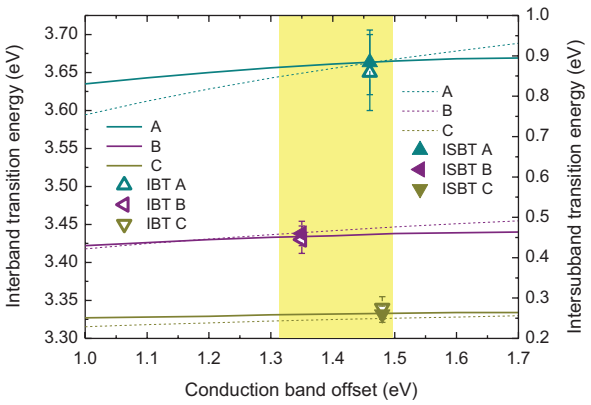

Figure 3 (online color at: www.pss-a.com) Calculated interband transition energy (left scale, full curves) and intersubband transition energy (right scale, dotted curves) for different CBOs in comparison to the experimental values (symbols) for the samples A, B, and C (see Table 1). The bars indicate the calculated variation of the transition energies for a variation of ±1 ML.

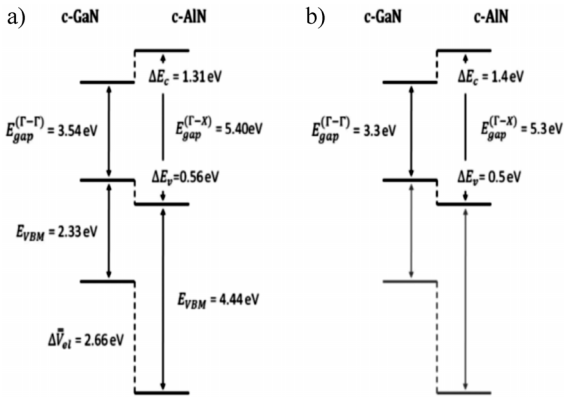

Figure 4 Schematic diagram of the band alignment between c-GaN and c-AlN, (a) calculated with *ab initio* and (b) experimental results.

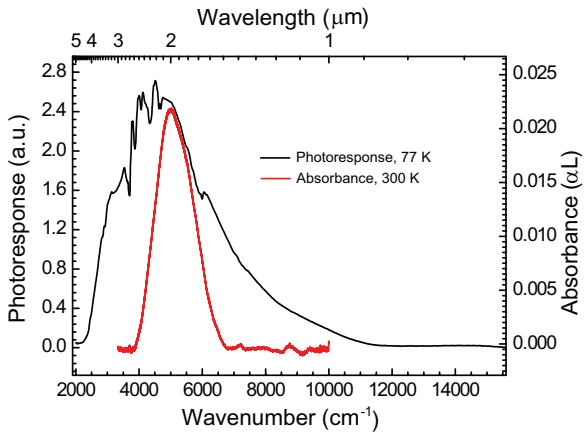

Figure 5 (online color at: www.pss-a.com) The photoresponse and optical absorbance spectra of a cubic GaN (1.6 nm)/AlN (1.44 nm) MQW with 20 periods measured at 77 and 300 K, respectively.

In this content it should be mentioned that for the calculations of the transition energies in cubic GaN/AlN superlattices the indirect band gap of c-AlN [13] should be used similar to the case of the more popular GaAs/AlAs superlattice [14].

3.4 Intersubband absorption in the 1.5 μm spectral range For intersubband transitions in the technologically important infrared 1.3–1.5 μm spectral range additional cubic GaN/AlN short period MQW structures were grown by using plasma-assisted MBE on free standing 3C-SiC substrates [15]. The buffer layer was 100 nm thick GaN and the active region was composed of 20 periods of L_W GaN/1.5 nm AlN, where L_W is the well thickness between 1.6 and 2.10 nm. The active region is then capped by a 100 nm thick GaN. The structural properties were checked by HRXRD. From the difference of the superlattice peaks in the ω–2Θ scan of the (002) reflection a periodicity of 3.1 nm was estimated by using a dynamic simulation program for a 20 period GaN/AlN MQW structure. From the knowledge of the growth rates of AlN and GaN, obtained from RHEED oscillations, a barrier and well width of 1.44 and 1.6 nm is determined, respectively. The optical absorption spectra of the intersubband transitions measured for all samples exhibit strong absorption peaks in the spectral range of 1.5−2 μm at room temperature [15].

Recently, photo-detectors based on intersubband transitions in molecular-beam epitaxially grown cubic GaN/AlN MQWs were fabricated and tested [16]. The samples were polished into waveguide configuration on which the devices were fabricated and the photo-response spectra were collected in the temperature range of 77–215 K under the influence of small bias voltages. All devices exhibit a photovoltaic effect where the photo-response is observed at zero bias voltage. Figure 5 shows both the optical absorbance and the photo-response at 77 K of a cubic 1.6/1.44 nm GaN/AlN short-period MQW at about 1.9 μm.

3.5 Intersubband absorption in the terahertz spectral range For GaN/$Al_xGa_{1-x}N$ QWs with low Al content x ISB absorption at THz frequencies may open prospects for the future development of quantum cascade lasers in this material system. Therefore in sample D (see Table 1) the AlN barrier material in the MQWs was replaced by an $Al_{0.05}Ga_{0.95}N$ barrier. The transmission measurements in the THz spectral region were performed at 4.7 K in a Bruker FTIR using a glow-bar source and a liquid helium-cooled Si bolometer. The sample was cut into two pieces of same length. Both pieces were polished with 30° facets and placed face to face under mechanical pressure on the cold finger of a liquid helium-cooled cryostat. This configuration allowed enhancing the light transmission by doubling the surface of the input facet. Placing the active QWs face to face also provides a good coupling of the TM-polarized THz radiation with the ISB transitions.

Figure 6 shows the transmission spectrum of sample D for TM- and TE-polarized light. The transmission of the sample has been normalized to one at low energies. Sample D exhibits an absorption peaked at 19.7 meV (4.76 THz) only for TM-polarized light, which is a clear signature of its ISB origin. The three unpolarized absorption resonances between 30 and 40 meV are related to the SiC-on-Si substrate. They appear only at low temperature and can be tentatively attributed to impurity absorption in SiC (shallow nitrogen donor absorption [17]).

3.6 Resonant tunneling A general understanding of resonant tunneling through cubic III-nitride double barrier structures is of crucial importance for optoelectronic devices like quantum well infrared detectors or quantum cascade lasers. Three different RTD (samples E, F, and G) were grown by PA-MBE on free standing n-type cubic silicon carbide. All RTDs consist of a highly doped 50 nm thick c-GaN buffer layer doped with silicon (Si). Doping concentration was 5×10^{19} cm^{-3} for all samples, respectively. The buffer layer is followed by the resonant tunneling

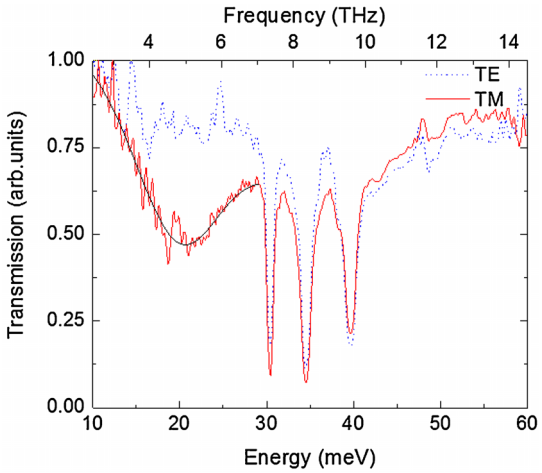

Figure 6 (online color at: www.pss-a.com) Low-temperature far-infrared transmission spectrum of sample D for TM- (red solid line) and TE- (blue dotted line) polarized light. Black solid line is a Gaussian fit of the absorption with a linear baseline.

structure. The tunneling structure consists of a 1 nm thick unintentionally doped (uid) c-GaN quantum well (QW) embedded in two Al(Ga)N barriers which are unintentionally doped as well. The barrier thickness was 3 nm for the sample with pure c-AlN barriers (sample E), and 1 and 2 nm for samples with $Al_{0.3}Ga_{0.7}N$ barriers (sample F and G), respectively. For more details see Ref. [5].

The *I*–*V*-characteristics of all three samples revealed a clear NDR in forward bias direction. The *I*–*V*-curves were asymmetrical as an effect of the heterojunction between 3C-SiC and c-GaN. No NDR could be observed in negative bias direction. In Fig. 7, the *I*–*V*-characteristics of samples E, F, and G are plotted for the first *I*–*V*-measurement. The current was normalized for better comparability. Overall PVRs from 2.7 to 1.3 are observed. For samples with AlGaN

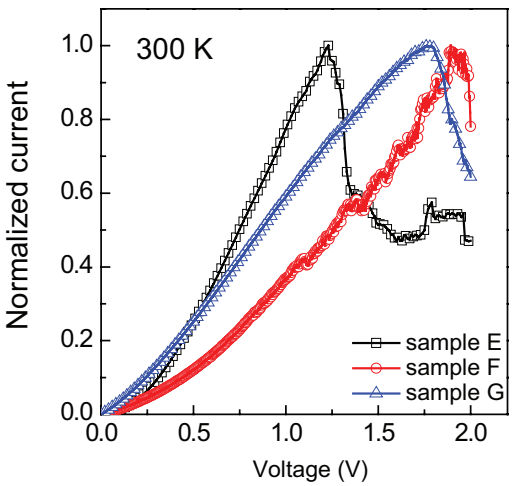

Figure 7 (online color at: www.pss-a.com) Typical *I*–*V*-characteristics of samples E, F, and G for the first measurement.

barriers the resonance peak occurs at higher bias voltage than for sample E, although for sample E the confinement energy is larger due to larger band offset between barriers and QW. This is an effect of higher contact resistances of the different samples since the contacts were not thermal annealed in order to avoid interdiffusion in the tunneling structure.

The tunneling characteristics have been modeled using nextnano[3]. The *I*–*V*-characteristics as well as electron densities were calculated using the contact block reduction method (CBR). More information about the theoretical model can be found in Ref. [18]. Only a small deviation of the peak voltage between calculation and experimental data is observed. These deviations may be due to leakage current through conducting channels or non-resonant tunneling which is not included in the calculation. Interface roughness and layer thickness fluctuations also influence the experimental results and lead to a broadening of the resonance peak. The calculated electron densities for three different bias voltages, below resonance, resonant tunneling, and off resonance are plotted in Fig. 8 together with the corresponding band structure. Only if the Fermi level is resonant with the localized state we find a remarkable density inside the quantum well. If bias voltage is further increased current transfer over the barrier structure occurs.

When measuring the *I*–*V*-characteristics we observed that the NDR vanishes after the first or second voltage sweep, which has been observed in the hexagonal system as well [19]. In order to find the physical origin of this behavior we have illuminated the sample with an UV-light, having its maximum intensity at a wavelength of 370 nm. After 1 h of UV-exposure the NDR could be recovered several times. The same behavior is found for other samples as well and is an indication for charge trapping as it is mentioned in Ref. [20] as well.

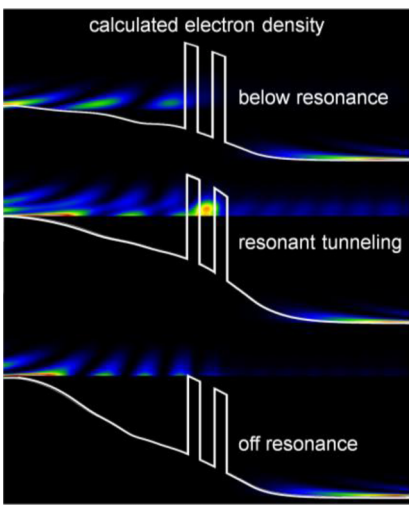

Figure 8 (online color at: www.pss-a.com) Calculated electron density and corresponding band structure for three different bias voltages. Resonant tunneling occurs for the case of high density inside the QW (middle).

4 Summary Recent developments of the *in situ* control of growth conditions during the MBE of cubic III-nitrides (GaN/AlN) paved the way to the production of layer stacks with high phase purity and severely improved structural properties. Cubic group III-nitride nanostructures are free of any polarization fields due to their cubic crystal symmetry and therefore may be considered as the true nonpolar group III-nitrides and thus are the ideal material basis of devices where polarization fields are detrimental for their performance. We performed an experimental and theoretical study of the ISB transitions in GaN/Al(Ga)N cubic quantum wells. The ISB absorption wavelength was tuned from 1.5 μm (telecommunication range) to 63 μm (THz frequency range). This corresponds to the shortest and the longest ISB wavelength ever achieved in this material system. Simulations of the quantum confinement in the framework of effective mass approximation allow us to refine material parameters. RTD with reproducible *I*–*V*-characteristics and recoverable NDR based on Al(Ga)N/GaN double barrier structures were fabricated. All devices show clear NDR with PVRs between 1.3 and 2.7. The observation of resonant tunneling and ISB absorption at 1.5 mm and at THz frequencies opens prospects for the future development of intersubband devices operating at non-cryogenic temperature in this material system.

Acknowledgements The authors want to thank Prof. K. Lischka, Prof. W.G. Schmidt, and E. Rauls at University of Paderborn, Prof. F. Julien, and M. Tchernycheva at University Paris-Sud, Prof. M.O. Manasreh, and E. DeCuir, Jr. at Arkansas State University. My special regards are expressed to Dr. H. Nagasawa at HOYA Corporation, for the supply of excellent 3C-SiC substrates and the financial supply by DFG (within the research group "Micro- and Nano-structures in Optoelectronics and Photonics" GRK 1464 and Project No. As (107/4-1)).

References

[1] D. J. As, Microelectron. J. **40**(2), 204 (2009).
[2] C. Mietze, M. Landmann, E. Rauls, H. Machhadani, S. Sakr, M. Tchernycheva, F. H. Julien, W. G. Schmidt, K. Lischka, and D. J. As, Phys. Rev. B **83**, 195301 (2011).
[3] J. Schörmann, S. Potthast, D. J. As, and K. Lischka, Appl. Phys. Lett. **89**, 131910 (2006).
[4] H. Machhadani, M. Tchernycheva, S. Sakr, L. Rigutti, R. Colombelli, E. Warde, C. Mietze, D. J. As, and F. H. Julien, Phys. Rev. B **83**, 075313 (2011).
[5] C. Mietze, K. Lischka, and D. J. As, Phys. Status Solidi A **209**(3), 439 (2012).
[6] T. Schupp, G. Rossbach, P. Schley, R. Goldhahn, M. Röppischer, N. Esser, C. Cobet, K. Lischka, and D. J. As, Phys. Status Solidi A **207**(6), 1365 (2010).
[7] O. Brandt, P. Waltereit, and K. H. Ploog, J. Phys. D **35**, 577 (2002).
[8] D. J. As, Proc. SPIE **7608**, 76080G (2010).
[9] A. Helman, M. Tchernycheva, A. Lusson, E. Warde, F. H. Julien, K. Moumanis, G. Fishman, E. Monroy, B. Daudin, L. S. Dang, E. Bellet-Amalric, and D. Jalabert, Appl. Phys. Lett. **83**, 5196 (2003).
[10] M. Tchernycheva, L. Nevou, L. Doyennette, F. H. Julien, E. Warde, F. Guillot, E. Monroy, E. Bellet-Amalric, T. Remmele, and M. Albrecht, Phys. Rev. B **73**, 125347 (2006).
[11] F. H. Julien, M. Tchernycheva, L. Nevou, L. Doyennette, R. Colombelli, E. Warde, F. Guillot, and E. Monroy, Phys. Status Solidi A **204**, 1987 (2007).
[12] T. Unuma, M. Yoshita, T. Noda, H. Sakaki, and H. Akiyama, J. Appl. Phys. **93**, 1586 (2003).
[13] M. Röppischer, R. Goldhahn, G. Rossbach, P. Schley, C. Cobet, N. Esser, T. Schupp, K. Lischka, and D. J. As, J. Appl. Phys. **106**, 076104 (2009).
[14] E. Finkman, M. D. Sturge, and M. C. Tamargo, Appl. Phys. Lett. **49**(19), 1299 (1986).
[15] E. A. DeCuir, Jr., E. Fred, M. O. Manasreh, J. Schörmann, D. J. As, and K. Lischka, Appl. Phys. Lett. **91**, 041911 (2007).
[16] E. A. DeCuir, Jr., M. O. Manasreh, E. Tschumak, J. Schörmann, D. J. As, and K. Lischka, Appl. Phys. Lett. **92**, 201910 (2008).
[17] C. Q. Chen, R. Helbiga, J. Zemanb, and A. J. L. Poulterb, Physica B **293**, 402 (2001).
[18] S. Birner, C. Schindler, P. Greck, M. Sabathil, and P. Vogl, J. Comput. Electron. **8**, 267 (2009).
[19] S. Golka, C. Pflügl, W. Schrenk, C. Skierbiszewski, M. Siekacz, I. Grzegory, S. Porowski, and G. Strasser, Appl. Phys. Lett. **88**, 172106 (2006).
[20] N. Zainal, S. V. Novikov, C. J. Mellor, C. T. Foxon, and A. J. Kent, Appl. Phys. Lett. **97**, 112102 (2010).